Σ-hypernuclear production in flight

Dean Halderson
Physics Department, Western Michigan University, Kalamazoo, Michigan 49008
(Received 2 June 1989)

Calculations for the in-flight production of Σ hypernuclei with the reactions $^{12}C(K^-,\pi^-)^{12}_{\Sigma}C$, $^{12}C(K^-,\pi^+)^{12}_{\Sigma}B$, $^{16}O(K^-,\pi^+)^{16}_{\Sigma}C$, and $^{9}Be(K^-,\pi^-)^{9}_{\Sigma}Be$ are presented. The framework of the recoil continuum shell model is employed. The calculations can account for the major feature of the data with a modification of the ΣN interaction of Yamamoto and Bando. This provides information on the strength of the central part of the ΣN interaction and on the $\Sigma N \rightarrow \Lambda N$ conversion strength. However, detailed information on the spin components of the ΣN force will be difficult to obtain.

I. INTRODUCTION

The experimental search for structure information on Σ hypernuclei has been somewhat frustrating. Experiments utilizing capture at rest initially showed encouraging results;[1,2] however, the structure that appeared in the first $^{12}C(K^-,\pi^+)^{12}_{\Sigma}Be$ data set is now thought to be statistical in origin.[3] A theoretical analysis of this reaction was reported in Ref. 4. In that paper two difficulties with the reaction were discussed: first, that the negatively charged Σ^- will not form narrow resonances, and second, that capture at rest produces a significant quasifree background. The paper concluded by suggesting that (K^-,π^-) in-flight experiments would provide a better opportunity to observe structure in Σ hypernuclei. The Σ^0 and Σ^+ produced in (K^-,π^-) will be more likely to produce sharp resonances, and with in-flight experiments one can make use of the energy dependence of the elementary interaction to separate excitations of different sigma charge states. In addition, one can make use of angular distributions as well as incident kaon energy to give control over the momentum transfer and therefore over the quasifree background.

This paper concludes the study which was begun in Ref. 4 by reporting on calculations for (K,π) in-flight cross sections. The wave functions were obtained with the formalism of the recoil corrected continuum shell model (RCCSM) and the hyperon-nucleon-Gaussian (YNG) interaction of Bando and Yamamoto.[5] Comparisons are made to data from the reactions $^{16}O(K^-\pi^-)^{16}_{\Sigma}C$, $^{12}C(K^-,\pi^-)^{12}_{\Sigma}C$, $^{12}C(K^-,\pi^+)^{12}_{\Sigma}Be$, and $^{9}Be(K^-,\pi^-)^{9}_{\Sigma}Be$. The YNG interaction appears to be slightly too strong to fit the existing data. Good fits to the carbon data are obtained with factors of 0.7 and 0.1 times the real and imaginary potentials, respectively. Fits to the oxygen and beryllium data are, however, less successful. The concentrated strength near sigma threshold, expected from the calculations, does not appear in the $p_K = 450$ MeV, $^{16}_{\Sigma}O$ data or the $p_K = 720$ MeV, $^{9}_{\Sigma}Be$ data. For beryllium the calculated peaks are not as narrow as those appearing in the data. These difficulties indicate a need for modifying the spin and range structure of the YNG interaction. However, due to the lack of sharp sigma states, it will be difficult to extract the spin structure from existing data.

II. THEORY

The formalism employed in this paper is that of the RCCSM.[6,7] The RCCSM generates hyperon wave functions in terms of internal coordinates by solving the translationally invariant Hamiltonian

$$H = H_{\text{core}} + p_{\Sigma}^2/2m + \sum_i V_{\Sigma N} - T_{\text{c.m.}} \ . \tag{1}$$

The distorted-wave cross section is given by

$$d\sigma/d\Omega = [J_i]^{-1} \sum_{M_i M_f} (2\pi/\hbar c)^4 (k_f/k_i) \times (\omega_K \omega_A \omega_\pi \omega_B/s) |T_{ba}|^2 \tag{2}$$

where

$$T_{ba} = \sum_n \int \chi_f^{(-)}[(M_A/M_B) r_{KA}] \Phi_B^*(X) v(r_n - r_{KA}) \times \Phi_A(X) \chi_i^{(+)}[r_{KA}] dX \, d^3 r_{KA} \ . \tag{3}$$

The initial nuclear spin is J_i, $[J_i] = 2J_i + 1$, A denotes the target nucleons, B denotes the hypernucleus, the ω's are total energies in the meson-nucleus center of mass, $s^{1/2}$ is the total meson-nucleus center-of-mass energy, and X is the set of internal baryon coordinates. The distorted waves, χ, for the kaons were obtained from local potentials which were generated[8,9] by folding the elastic t matrices of Gopal *et al.*[10] For pions with over 310 MeV of laboratory kinetic energy, the distorted waves were obtained from local potentials which were generated by folding the elastic t matrices of Davies.[11] For pions with under 310 MeV of laboratory kinetic energy, the distorted waves were generated with the kinematics used by Stricker, McManus, and Carr,[12] but with b_0, b_1, c_0, and c_1 obtained directly from the phase shifts in Ref. 2 of Ref. 12. The transition operator in Eq. (2) is taken as the elementary $KN \rightarrow \pi\Sigma$ t matrix from Ref. 10. All of the elementary t matrices have been Fermi averaged over the momentum distribution of the struck nucleon in the method of Ref. 13.

III. RESULTS

Calculations for the (K,π) reaction leading to Σ hypernuclei have been performed by other authors.[14–19] The advantages of the RCCSM are its ability to include bound states and resonances in a consistent framework and to obtain configurations free of spurious center-of-mass excitations from a realistic two-body interaction. In addition, the RCCSM allows use of a complex, spin-dependent ΣN interaction. The complex interaction is one way to account for the $\Sigma N \rightarrow \Lambda N$ conversion process. It is not a completely correct procedure since, as pointed out in Ref. 4, it would correspond to observing the outgoing pion and an escaping sigma. However, the procedure does provide a mechanism for giving conversion widths to the sigma states.

A second procedure for giving conversion widths to the sigma states was discussed and demonstrated in Ref. 4. This second procedure was the use of effective lambda channels. These channels could be used to produce reasonable conversion widths. An example of this method is shown in Fig. 1 where the 1° cross section for $^{12}C(K^-,\pi^+)^{12}_{\Sigma}Be$, calculated with effective Λ channels at $p_{\bar{K}}=450$ MeV/c, is compared with the forward-angle data of Ref. 20. The $^{12}_{\Sigma}Be$ wave functions are from Ref. 4. When compared to data, all theoretical curves in this work have been folded with a Gaussian of 1.0 MeV width to simulate detector resolution. The fit looks very good, and the 2.27 multiplicative factor applied to the data could easily be argued away by uncertainties in distorting potentials or in data normalization. However, since the effective channels did not correspond to the dominant physical channels, there was no theoretical guide for setting the thresholds of the effective channels and the strength of the $\Sigma N \rightarrow \Lambda N$ interaction in those channels. Therefore, in the calculations that follow, the conversion widths will be included by use of a complex two-body interaction, which can be related to the self-energy of the sigma in nuclear matter.

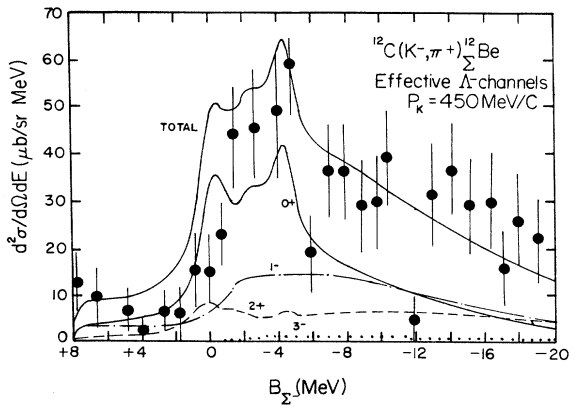

FIG. 1. The forward $^{12}C(K^-,\pi^+)^{12}Be$ cross section. Data are from Ref. 20 and have been multiplied by a factor of 2.27. Calculation is a 1° and includes the real YNG potential at $k_F=0.8$ fm^{-1}, and effective lambda channels. The calculations were folded with a 1 MeV Gaussian.

The complex interaction provided by Ref. 5 is density dependent. This poses a problem for the RCCSM which relies on a translationally invariant Hamiltonian. Density dependences can be incorporated in the RCCSM via Skyrme-type interactions, but not those that rely on variation of the potential as a function of distance from a point fixed in space. Therefore the question arises as to which density is most appropriate for the RCCSM calculation. To provide some guidance, one can look at local equivalent sigma potentials obtained by folding the density-dependent interaction. If one neglects the sigma-nucleon mass difference, the central part of the spin-averaged ΣN interaction can be put in the form

$$V_{\Sigma N}=V_0+V_\tau \mathbf{t_N}\cdot\mathbf{T_\Sigma}+(V_X+V_{X\tau}\mathbf{t_N}\cdot\mathbf{T_\Sigma})P_X\ , \tag{4}$$

where

$$V_0=({}^1E_{1/2}+{}^1O_{1/2}+3{}^3E_{1/2}+3{}^3O_{1/2}+2{}^1E_{3/2}+2{}^1O_{3/2}+6{}^3E_{3/2}+6{}^3O_{3/2})/24\ , \tag{5}$$

$$V_\tau=(-{}^1E_{1/2}-{}^1O_{1/2}-3{}^3E_{1/2}-3{}^3O_{1/2}+{}^1E_{3/2}+{}^1O_{3/2}+3{}^3E_{3/2}+3{}^3O_{3/2})/12\ , \tag{6}$$

$$V_X=({}^1E_{1/2}-{}^1O_{1/2}+3{}^3E_{1/2}-3{}^3O_{1/2}+2{}^1E_{3/2}-2{}^1O_{3/2}+6{}^3E_{3/2}-6{}^3O_{3/2})/24\ , \tag{7}$$

$$V_{X\tau}=(-{}^1E_{1/2}+{}^1O_{1/2}-3{}^3E_{1/2}+3{}^3O_{1/2}+{}^1E_{3/2}-{}^1O_{3/2}+3{}^3E_{3/2}-3{}^3O_{3/2})/12\ , \tag{8}$$

and ${}^SP_T$ stands for singlet or triplet, even or odd, $T=\frac{1}{2}$ or $\frac{3}{2}$.

The direct and exchange contributions to the folded potentials and given by[21]

$$V^D(r_0)=\int\{V_0[r,\rho(\tfrac{1}{2}|\mathbf{r}_1+\mathbf{r}_0|)]\rho(\mathbf{r}_1)-\tfrac{1}{2}q_\Sigma V_\tau[r,\rho(\tfrac{1}{2}|\mathbf{r}_1+\mathbf{r}_0|)][\rho_n(r_1)-\rho_p(r_1)]\}dr_1 \tag{9}$$

and

$$V^E(r_0)=\int\{V_X[r,\rho(\tfrac{1}{2}|\mathbf{r}_1+\mathbf{r}_0|)]\rho(\tfrac{1}{2}|\mathbf{r}_1-\mathbf{r}_0|)-\tfrac{1}{2}q_\Sigma V_{X\tau}(r,\rho[\tfrac{1}{2}(\mathbf{r}_1+\mathbf{r}_0)]) \times(\rho_n(\tfrac{1}{2}|\mathbf{r}_1+\mathbf{r}_0|)-\rho_p[\tfrac{1}{2}(\mathbf{r}_1+\mathbf{r}_0)])\}S(k_Fr)j_0(kr)dr\ , \tag{10}$$

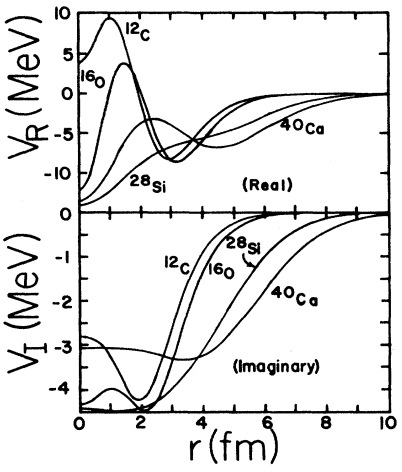

FIG. 2. Folded potentials for a 2.0 MeV Σ^0. All calculations include the density dependence of the YNG interaction.

where $\mathbf{r}_1$ locates a point in the nucleus from its center, $\mathbf{r}=\mathbf{r}_1-\mathbf{r}_0$, $k_F=3/2\pi^2\rho[\frac{1}{2}(\mathbf{r}_1+\mathbf{r}_0)]$, $S(x)=3j_1(x)/x$, and k is taken as the asymptotic momentum $k^2=2mE_\Sigma/\hbar^2$. The choice of an asymptotic or local momentum approximation makes little difference in what follows.

The potentials for a 2.0 MeV Σ^0 scattering from ^{12}C, ^{16}O, ^{28}Si, and ^{40}Ca are shown in Fig. 2. One sees a rather unusual shape to the potential, much like those calculated in Ref. 22 for bound states. The shape is due to the

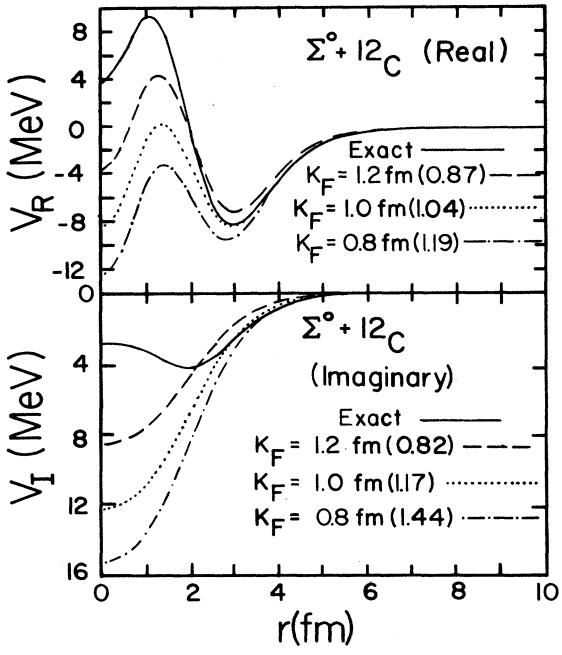

FIG. 3. Folded potentials for $\Sigma^0+^{12}C$ with constant k_F as compared with the density-dependent potential. The numbers in parentheses are the ratios of the constant-density potential volume integrals to the variable-density potential volume integral.

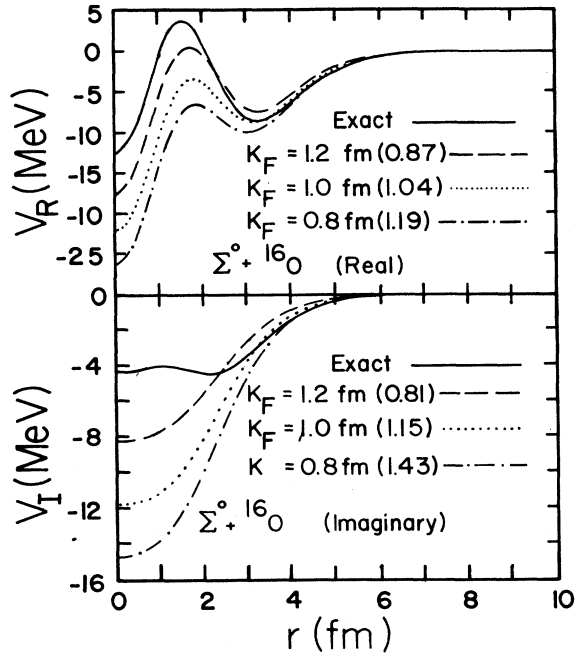

FIG. 4. Folded potentials for $\Sigma^0+^{16}O$ with constant k_F as compared with the density-dependent potential. The numbers in parentheses are the ratios of the constant-density potential volume integrals to the variable-density potential volume integral.

sensitive cancellation of the direct and exchange terms, whose shapes themselves are very sensitive additions of the different partial waves of the potential. The physical significance of the folded potentials is quite limited, but they are useful for comparing to potentials obtained with constant k_F. In Figs. 3 and 4 are again plotted the density-dependent potential for ^{12}C and ^{16}O along with the potentials calculated with $k_F=0.8$, 1.0, and 1.2 fm^{-1}. One sees that none of the density-independent calculations can reproduce the density-dependent ones. In parentheses for each curve is the ratio of the potential volume to the volume of the density-dependent potential.

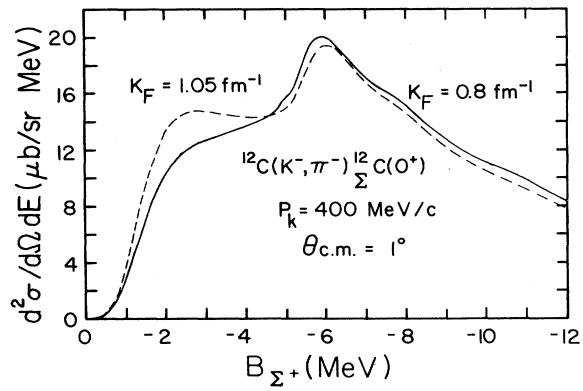

FIG. 5. Calculated $\theta_{c.m.}=1°$ cross sections for $^{12}C(K^-,\pi^-)^{12}_\Sigma C(0^+)$ for $k_F=0.8$ and 1.05 fm^{-1}. No Gaussian folding width is included.

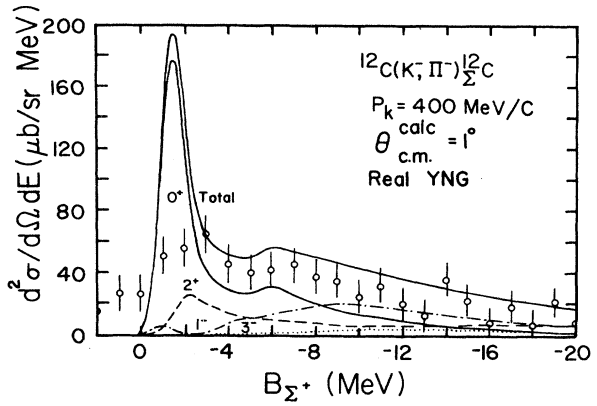

FIG. 6. Forward cross section for $^{12}C(K^-,\pi^-)^{12}_{\Sigma}C$ at $p_K=400$ MeV/c. The data from Ref. 25 have been arbitrarily normalized. Calculation includes real part of the YNG interaction.

Potentials calculated with $k_F=1.05$ fm^{-1} will approximately reproduce the density-dependent volume integrals for both ^{12}C and ^{16}O. Therefore this value will be used in the present calculations instead of 0.8 fm^{-1} used in Ref. 4. The difference between various choices of k_F is demonstrated in Fig. 5 for 0^+ excitation in $^{12}C(K^-,\pi^-)^{12}_{\Sigma}C$ at 400 MeV/c without folding with the 1 MeV Gaussian. The calculations show some differences, but retain similar basic features. Of all the sigma-hypernuclear spectra available to date, these present calculations indicate that $^{12}C(K^-,\pi^-)^{12}_{\Sigma}C$ at 400 and 450 MeV/c hold the most hope for extracting some sort of structure information. Therefore it will be examined first and in some detail.

The complete calculations of $^{12}C(K^-,\pi^-)^{12}_{\Sigma}C$ at $p_K=400$ MeV/c are shown in Figs. 6 and 7 for a real and complex interaction, respectively (this work also includes the tensor ΣN interaction of Ref. 23). The basis for $^{12}_{\Sigma}C$ includes $\Sigma^0\times^{11}C(\frac{3}{2}^-,\frac{1}{2}^-,\frac{5}{2}^-,\frac{3}{2}^-)$ and $\Sigma^+\times^{11}B(\frac{3}{2}^-,\frac{1}{2}^-,\frac{5}{2}^-,\frac{3}{2}^-)$, where the ^{11}C and ^{11}B states are from Cohen and Kurath.[24] In Fig. 6 one notes that the background is suppressed and the 0^+ strength is the dominant feature of the cross section. This demonstrates one advantage of being able to work at a low momentum transfer with in-flight experiments. The calculated 0^+ spectrum with no absorption shows two distinct peaks. The peaks in this calculated cross section are genuine resonances and correspond to a lower state which is predominantly a Σ^+ excitation and an upper state which is predominantly a Σ^0 excitation.

The first state appears to be too strong and the ratio of peak heights is incorrect, however, when compared to the data.[20,25] For the comparison a background has been subtracted from the data. Adding the full YNG absorption changes the ratio of peak heights as shown in Fig. 7, and, in fact, changes it too much. The shape of the theoretical curve is not only dependent on the strength of the absorption (which only acts in the two-body ΣN, $T=\frac{1}{2}$ channel), but also on the strength of the real part of the YNG interaction and the strength of the mixing between Σ^+ and Σ^0 states. The mixing between Σ^+ and Σ^0 states is quite strong with the full YNG interaction. It produces a 0^+ substitutional state which is 90% $T=\frac{1}{2}$ as opposed to 67% for a pure Σ^+ state. Dover, Gal, and Millener[26] have argued that the (K^-,π^-) data support such a nearly pure isospin state. Because of the sensitivity of the Σ^+ and Σ^0 substitutional state peak heights and widths to the interaction and conversion strengths, an improved experimental spectrum would provide information on the strengths of $V_{\Sigma N}$ and $V_{\Sigma N\to\Lambda N}$.

Although the exact positions and widths of the peaks in the data cannot be taken seriously, it is possible to obtain a reasonable fit to their positions and apparent widths by scaling the real and imaginary parts of the two-body interaction by 0.7 and 0.1, respectively. (It would perhaps be more appropriate to decrease the coupling between the Σ^+ and Σ^0 channels; however, this would have meant altering the various components of the force with no theoretical guidance and the restriction of conserving isospin.) These $p_K=400$ MeV/c results are shown in Fig. 8. The results of the same calculation at $p_K=450$ MeV/c are shown in Fig. 9. Both the data and the calculated results show the increased excitation of the Σ^0 state over the Σ^+ state in going from 400 to 450

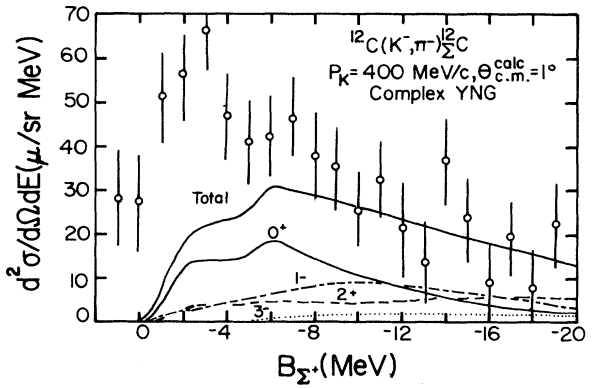

FIG. 7. Same as Fig. 6, but calculation includes complex YNG interaction.

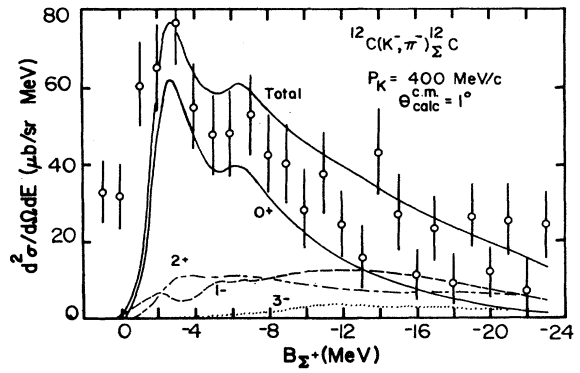

FIG. 8. Same as Fig. 6, but calculation includes a real scale factor of 0.7 and an imaginary scale factor of 0.1.

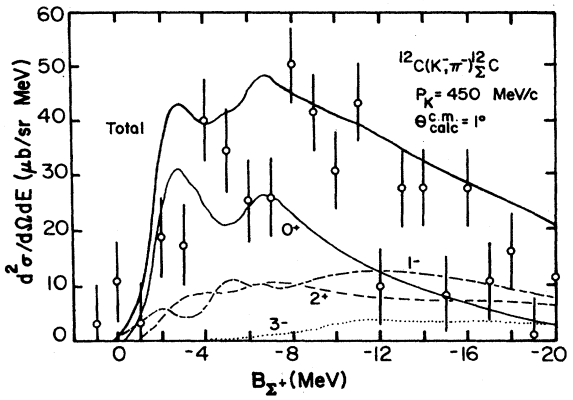

FIG. 9. Forward cross section for $^{12}C(K^-,\pi^-)^{12}_{\Sigma}C$ at $p_K=450$ MeV/c. Data are from Ref. 25. Calculation includes a real scale factor of 0.7 and an imaginary scale factor of 0.1.

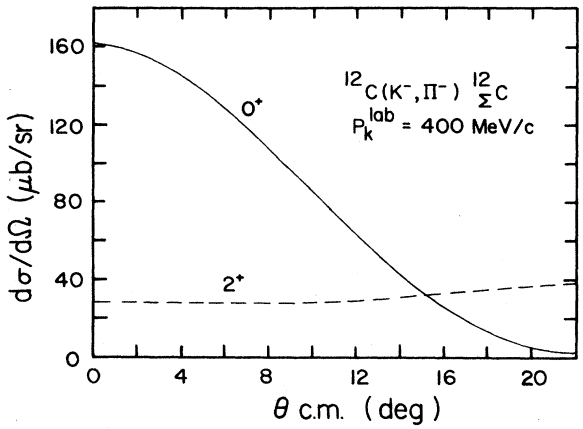

FIG. 11. Angular distributions for the first 0^+ and 2^+ resonances in Fig. 9.

MeV/c. As suggested in Ref. 25, this would be expected from the Fermi-averaged, elementary, center-of-mass cross section shown in Fig. 10. The behavior gives confirmation to the interpretation of the two peaks as Σ^0 and Σ^+ excitations and also confirms that the two-peak structure in the experimental $^{12}C(K^-,\pi^-)^{12}_{\Sigma}C$ cross section is real.

The chance of directly observing the spin-orbit component of $V_{\Sigma N}$ is less promising, because the substitutional states lie above threshold. For instance, if the $p_{3/2}-p_{1/2}$ spin-orbit splitting were large enough to be observed experimentally, then the escape width for the upper state would be too large to be located. Some chance does exist for observing the influence of the spin-dependent component of the ΣN interaction. The YNG interaction predicts a separation of the $|p_{3/2}\times^{11}B;(0^+)\rangle$ state and the $|p_{3/2}\times^{11}B;(2^+)\rangle$ state. This can be seen in Fig. 6, but certainly could not be distinguished in a 0° experimental spectrum. However, Fig. 11 shows the angular dependence of the cross sections for the integrated peaks in Fig. 9. Here it is seen that the 2^+ state will dominate at 22°. Therefore, if the resonances are narrow enough, which from the data of Ref. 25, it appears they could be, the position of the 2^+ resonance could be located from the 22° spectrum and the 0^+-2^+ splitting determined.

Normalized experimental cross sections are available for $^{12}C(K^-,\pi^+)^{12}_{\Sigma}Be$ at 450 MeV/c.[20] The $^{12}_{\Sigma}Be$ basis included in the present work consists of

$$\Sigma^-\times^{11}B(\tfrac{3}{2}^-,\tfrac{1}{2}^-,\tfrac{5}{2}^-,\tfrac{3}{2}^-)$$

and

$$\Sigma^0\times^{11}Be(\tfrac{1}{2}^+,\tfrac{1}{2}^-,\tfrac{5}{2}^+,\tfrac{3}{2}^-)\ ,$$

where the ^{11}B wave functions are from Ref. 24 and the ^{11}Be wave functions are from Ref. 27. Calculations with the YNG force adjusted as above are compared to these data in Fig. 12. The shape of the cross and the magnitude are reasonably well reproduced for this purely $T=\frac{3}{2}$ excitation. However, as explained in Ref. 4 for the calculations for stopped kaons, the peaks in the $^{12}_{\Sigma}Be(0^+)$ spectrum are just p-wave strength which is modulated by threshold effects. Similar results for this reaction were obtained in Ref. 10. Therefore, even though the

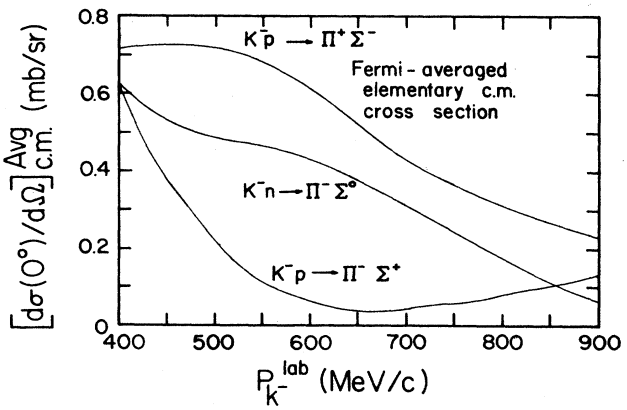

FIG. 10. Center-of-mass cross section for $KN\rightarrow\pi\Sigma$, Fermi averaged over a p-state momentum distribution.

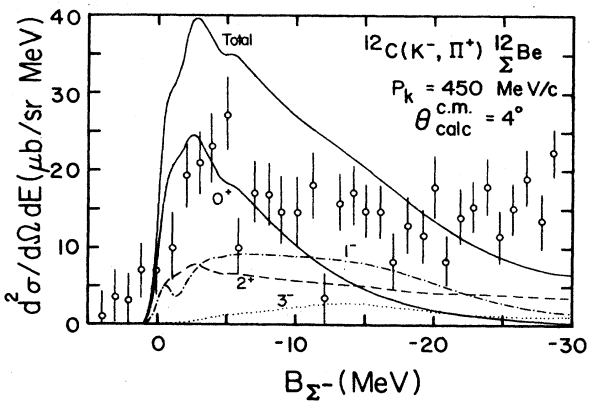

FIG. 12. The forward $^{12}C(K^-,\pi^+)^{12}_{\Sigma}Be$ cross section at $p_K=450$ MeV/c. Data are from Ref. 20. Calculation is at $\theta_{c.m.}=4°$ and includes the potential scale factors of 0.7 and 0.1.

(K^-,π^+) reaction was very attractive because it places only a Σ^- in the nucleus, this negatively charged particle leads to an extremely large escape width. This demonstrates the difficulty of trying to investigate Σ hypernuclei via (K^-,π^+). Little structure information would be gained by pursuing a better experimental spectrum in this case. Indeed, the new Brookhaven data[28] with better statistics at $p_K=715$ MeV/c showed no useful structure.

A comparison with these 715 MeV/c data at 4° is shown in Fig. 13(a) where one sees that the shape of the data is reproduced, but not the magnitude. In fact one sees that the experimental cross section must be divided by a factor of 4.5. The 12° data are shown in Fig. 13(b) with the same scale factor. It is true that one has little confidence in the high-energy kaon and pion optical potentials for this momentum. The impulse approximation does not fit the existing data very well and too little data are available for global fits. (Acquiring such data would appear less than exciting, but may yield important physics.) This makes it difficult to comment on the physical significance of the disagreement in magnitudes. However, one can compare with other high-momentum data for which normalized cross sections are available.[20] Shown in Fig. 14 is the $^{16}O(K^-,\pi^+)^{16}_{\Sigma}C$ at $p_K=713$ MeV. Here one sees that the data require only division by a factor of 2. It would be difficult to see how such a drastic change in the quality of the theoretical results could occur between ^{16}O and ^{12}C. It would most likely mean a difficulty in the normalization of the experimental cross sections.

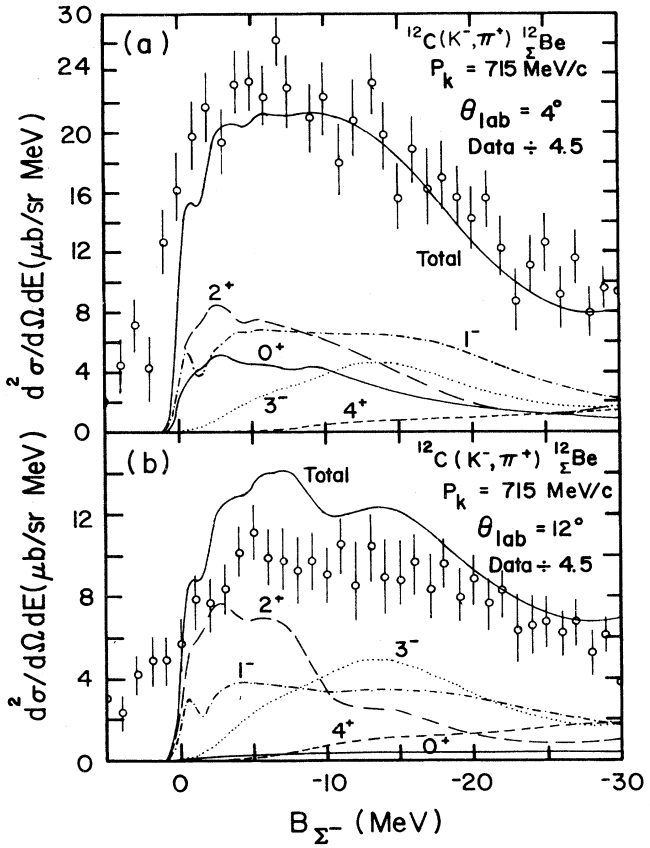

FIG. 13. Cross section for $^{12}C(K^-,\pi^+)^{12}_{\Sigma}Be$ with $p_K=715$ MeV/c at (a) $\theta_{lab}=4°$ and (b) $\theta_{lab}=12°$. The data from Ref. 28 have been divided by a factor of 4.5. The calculations include the potential scale factors of 0.7 and 0.1.

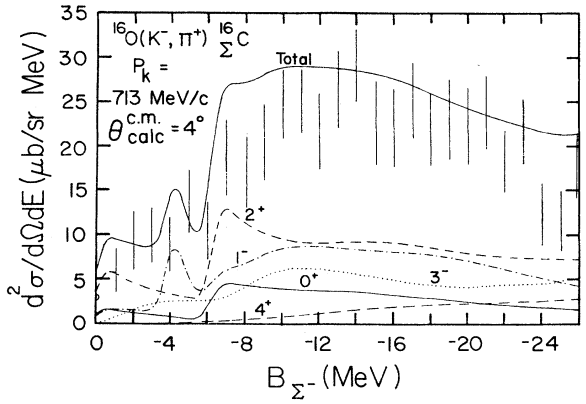

FIG. 14. Forward cross section for $^{16}O(K^-,\pi^+)^{16}_{\Sigma}C$ at $p_K=713$ MeV/c. Data are from Ref. 20. Calculation is at $\theta_{c.m.}=4°$ and includes the potential scale factors of 0.7 and 0.1. Data have been divided by 2.1.

The next calculation is for $^{16}O(K^-,\pi^+)^{16}_{\Sigma}C$ at 450 MeV. This is the most puzzling of the experimental cross sections.[20] In Fig. 15 one can see that the shape of the cross section is not reproduced. The main question is whether there is really a dip at $B_{\Sigma^-}=-8.0$ MeV. The optical-model calculations of Ref. 17 show no dip because they do not solve the coupled-channels, structure problem. The present calculation shows a dip, but in the wrong place. The dip in the calculation occurs because of an interference in the $p^{-1}_{1/2}-p^{1/2}$ and the $p^{-1}_{3/2}-p_{3/2}$ amplitudes and because of the characteristic threshold rises that correspond for an unbound Σ^-. Figure 16 demonstrates these rises for the 0^+ cross section without folding with a 1 MeV Gaussian. This shape has been reported in other types of continuum calculations.[19]

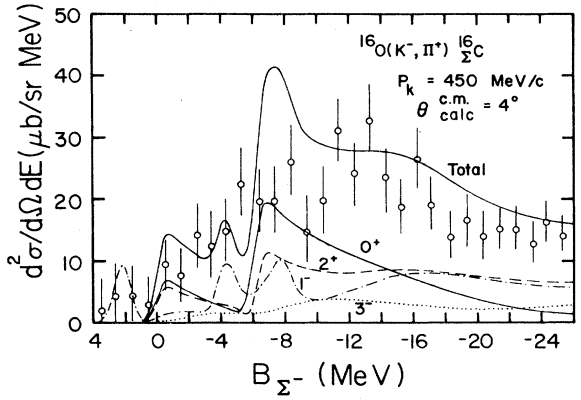

FIG. 15. Forward cross section for $^{16}O(K^-,\pi^+)^{16}_{\Sigma}C$ at $p_K=450$ MeV/c. Data are from Ref. 20. Calculation is at $\theta_{c.m.}=4°$ and includes the potential scale factors of 0.7 and 0.1.

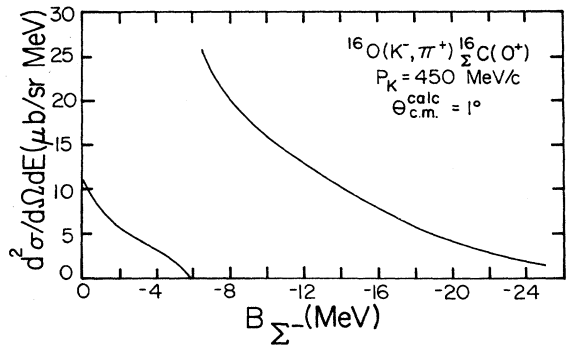

FIG. 16. Cross section for $^{16}O(K^-,\pi^+)^{16}_{\Sigma}C(0^+)$ at $\theta_{c.m.}=4°$ and $p_K=450$ MeV/c. No Gaussian folding width is included.

The final spectrum is $^9Be(K^-,\pi^-)^9_{\Sigma}Be$ at $p_K=720$ MeV/c, shown in Fig. 17.[29] This spectrum has been a puzzle because of the two peaks at $B_{\Sigma}0=-11$ and -23 MeV. Similar peaks have appeared in $^9_{\Lambda}Be$ and were explained as due to excitation of the $^8Be(2^+)\times p_{\Lambda}$.[30] However, similar calculations for $^9_{\Sigma}Be$ were not successful.[15] It has been speculated[15] that the peaks could correspond to excitations of the $\Sigma^+\times^8Li$ and $\Sigma^0\times^8Be$ channels, which may combine with $\Sigma\times^8B$ components to give states of reasonably good isospin. Therefore this work includes the $\Sigma^0\times^8Be(0^+:0,2^+:0,2^+:1,1^+:1,3^+:1)$, $\Sigma^+\times^8Li(2^+,1^+,3^+)$, and $\Sigma^-\times^8B(2^+,1^+,3^+)$ channels in the basis. The core states are from Cohen and Kurath.[24] In Fig. 17 one can see two peaks in the calculation, but they occur at -5 and -19 MeV and are not as narrow as the experimental peaks. The first calculated peak is due to excitation of Σ^0, s and p states coupled to the ^8Be, $T=0$ cores. The second calculated peak is primarily due to Σ^0, s and p states coupled to the ^8Be, $T=1$ cores, Σ^0, d states coupled to the ^8Be, $T=0$ cores, and Σ^+, s states coupled to the ^8Li cores.

It is instructive to look at one spin excitation separately. In Fig. 18 is plotted the $J=\frac{3}{2}^+$, J_T (transferred angular momentum) $=1^-$ contribution without folding in a 1 MeV Gaussian. The structures in this spectrum are strong threshold effects at the opening of the ^8Be, $T=0$

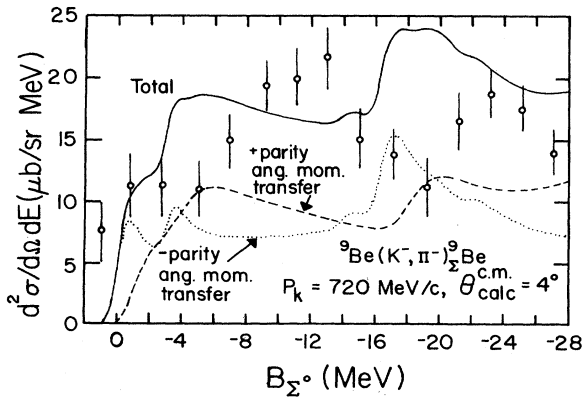

FIG. 17. Forward cross section for $^9Be(K^-,\pi^-)^9_{\Sigma}Be$ at $p_K=720$ MeV/c. Data are from Ref. 29. Calculation is at $\theta_{c.m.}=4°$ and includes the potential scale factors of 0.7 and 0.1.

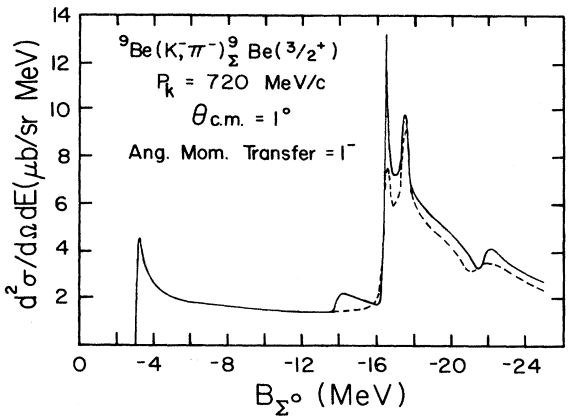

FIG. 18. Calculated cross section for $^9Be(K^-,\pi^-)^9_{\Sigma}Be(J=\frac{3}{2}^+,J_T=1)$ at $p_K=720$ MeV/c. Solid curve includes Σ^+ and Σ^0 excitations. Dashed curve results from suppression of Σ^+ excitations.

and ^8Be, $T=1$ channels, and are not due to resonances with identifiable isospin. The dashed line in the figure shows the results when Σ^+ production is set to zero, and demonstrates that Σ^+ production is not negligible even though one would expect little Σ^+ production from the elementary amplitudes in Fig. 10.

IV. DISCUSSION

Because of the disagreement between experimentally determined and calculated peak positions and widths in $^9_{\Sigma}Be$, one could not say that the above analysis of that calculation describes the actual structure of the experimental peaks. It would be possible to shift the peaks to higher energy by weakening the interaction; however, it would not be possible to reduce the calculated widths. Such a reduction would require altering the individual components of the real part of the interaction so as to deepen the effective single-particle well near the surface and decrease the well in the interior, to obtain a shape much like the density-dependent well in Fig. 3 for ^{12}C. Likewise, in $^{16}_{\Sigma}C$, the calculation could be made to look more like those data by weakening the interaction, but the dip position would still not be in agreement with the data.

In addition to exercising some caution on accepting the calculated structure as fact, one must also exercise some caution on interpreting the potential scaling coefficients. For instance, the imaginary scale factor of 0.1 could be construed as evidence that Σ-hypernuclear widths are ten times smaller than predicted from the elementary $\Sigma M\rightarrow\Lambda N$ conversion process. However, from the spectra used to determine the imaginary scale factor shown in Fig. 6, one can see that the two peaks retain their identity even with the full YNG absorption. It was not the widths that required narrowing, but the ratio of the peak heights that required adjustment. That ratio was a function of their structure and therefore a function of real interaction as well as the imaginary interaction. It would certainly be possible to increase the imaginary scale factor and still obtain reasonable fits to the data shown in

this paper. However, given the amount and quality of the existing data, such a fitting procedure is not justified. Before a comprehensive theoretical analysis could be made, the experiments must have improved resolution, the $M_Y - M_N$ scales must be known precisely, cross sections must be available at a variety of incident momenta, angular distributions must be available, and the cross sections must be properly normalized.

The question arises as to whether such an experimental effort is justified, or should one be satisfied with a qualitative measure of the strength of the ΣN interaction. The present work suggests that the necessary experimental effort is too difficult for presently available kaon beam intensities. However, if intensities can be increased by a factor of 10 in new or existing facilities, then new experiments could be justified. Indeed, the exploration of the baryon-baryon interaction remains a primary task of nuclear physics research. And even though the sigma states lie in the continuum, the techniques of the RCCSM can connect continuum state excitations directly to the two-body interaction just as precisely a bound-state shell model is related to bound-state structure.

V. CONCLUSION

Calculations for in-flight production of Σ hypernuclei have been carried out with the YNG interaction and in the framework of the RCCSM. A comparison of local, single-particle potentials with the density dependence included in the YNG interaction and those generated at a fixed density indicated that a fixed value of $k_F = 1.05$ fm^{-1} produced a single-particle potential volume equal to that of the density-dependent interaction. The YNG interaction at $k_F = 1.05$ fm^{-1} was then found to be too strong to fit existing cross sections. However, with real and imaginary scale factors of 0.7 and 0.1, respectively, one was able to obtain reasonable agreement with the cross sections of the mass-12 systems and the 730 MeV/c, ^{16}O$(K^-,\pi^+)^{16}_{\Sigma}$C cross sections, but the 450 MeV/c, ^{16}O$(K^-,\pi^+)^{16}_{\Sigma}$C data and the 720 MeV/$c$, ^{9}Be$(K^-,\pi^-)^{9}_{\Sigma}$Be data were poorly fitted. The peak locations and widths did not match the data.

The result that the full YNG interaction was too strong to fit existing cross sections indicates that one must look at other methods of converting the Nijmegen Model D potential[31] into a form for shell-model calculations or look at other potentials such as the Bonn potential.[32] It may also be necessary to include a three-body contribution to the interaction which would account for the density dependence in a manner that is useful in translationally invariant calculations. However, to go from a realistic YN potential to RCCSM generated cross section is quite arduous and the quality of present data does not warrant such an effort.

[1] T. Yamazaki *et al.*, Phys. Rev. Lett. **54**, 102 (1985).

[2] R. S. Hayano *et al.*, in *Proceedings of the 1986 INS International Symposium on Hypernuclear Physics,* edited by H. Bando, O. Hashimoto, and K. Ogawa (Insitute for Nuclear Study, Tokyo, 1986) p. 19.

[3] S. Paul *et al.*, Nucl. Phys. **A479**, 137c (1988).

[4] D. Halderson and R. J. Philpott, Phys. Rev. C **37**, 1104 (1988).

[5] Y. Yamamoto and H. Bando, Prog. Theor. Phys. Suppl. **81**, 9 (1985).

[6] R. J. Philpott, Nucl. Phys. **A289**, 109 (1977).

[7] D. Halderson, Phys. Rev. C **30**, 941 (1984).

[8] D. Halderson, P. Ning, and R. J. Philpott, Nucl. Phys. **A458**, 605 (1986).

[9] D. Halderson, M. Mo, and P. Ning, Phys. Rev. Lett. **57**, 1117 (1986).

[10] G. P. Gopal, R. T. Ross, A. J. Van Horn, A. C. McPherson, E. F. Clayton, T. C. Bacon, and I. Butterworth, Nucl. Phys. **B119**, 362 (1977).

[11] A. T. Davies, Nucl. Phys. **B21**, 359 (1970).

[12] K. Stricker, H. McManus, and J. A. Carr, Phys. Rev. C **19**, 929 (1979).

[13] A. S. Rosenthal and F. Tabakin, Phys. Rev. **22**, 711 (1980).

[14] J. Zofka, in *Proceedings of the 1986 INS International Symposium on Hypernuclear Physics,* edited by H. Bando, O. Hashimoto, and K. Ogawa (Institute for Nuclear Study, Tokyo, 1986), p. 97.

[15] O. Morimatsu and K. Yazaki, in *Proceedings of the 1986 INS International Symposium on Hypernuclear Physics,* edited by H. Bando, O. Hashimoto, and K. Ogawa (Institute for Nuclear Study, Tokyo, 1986), p. 50.

[16] K. Ikeda and T. Yamada, in *Proceedings of the 1986 INS International Symposium on Hypernuclear Physics,* edited by H. Bando, O. Hashimoto, and K. Ogawa (Institute for Nuclear Study, Tokyo, 1986), p. 59.

[17] M. Kohno, R. Hausmann, P. Siegel, and W. Weise, Nucl. Phys. **A470**, 609 (1987).

[18] R. Hausmann, Nucl. Phys. **A479**, 247c (1988).

[19] R. Wünsch and J. Zofka, Phys. Lett. B **193**, 7 (1987).

[20] T. Walcher, Nucl. Phys. **A479**, 63c (1988).

[21] F. A. Brieva and J. R. Rook, Nucl. Phys. **A291**, 317 (1977).

[22] M. Kohno, Prog. Theor. Phys. **78**, 123 (1987).

[23] C. B. Dover, A. Gal, L. Klieb, and D. J. Millener, Phys. Rev. Lett. **56**, 119 (1986).

[24] S. Cohen and D. Kurath, Nucl. Phys. **73**, 1 (1965).

[25] R. Bertini *et al.*, Phys. Lett. **136B**, 29 (1984).

[26] C. B. Dover, A. Gal, and D. J. Millener, Phys. Lett. **138B**, 337 (1984).

[27] W. D. Teeters and D. Kurath, Nucl. Phys. **A275**, 61 (1975).

[28] L. Tang *et al.*, Phys. Rev. C **38**, 846 (1988).

[29] R. Bertini *et al.*, Phys. Lett. **90B**, 375 (1980).

[30] T. Yamada, K. Ikeda, H. Bando, and T. Motoba, Phys. Lett. B **172**, 149 (1986).

[31] J. M. Nagels, T. A. Rijken, and J. J. deSwart, Phys. Rev. D **12**, 744 (1975); **15**, 3547 (1977); **20**, 1633 (1979).

[32] R. Machleidt, K. Holinde, and Ch. Elster, Phys. Rep. **149**, 1 (1987).